JOURNAL OF MATERIALS SCIENCE 28 (1993) 2615–2631

Si–C–N ceramics with a high microstructural stability elaborated from the pyrolysis of new polycarbosilazane precursors

Part I *The organic/inorganic transition*

D. MOCAER, R. PAILLER, R. NASLAIN
Laboratoire des Composites Thermostructuraux (UMR-47 CNRS-SEP-UB1), Domaine Universitaire, 3 Allée de la Boëtie, F-33600, Pessac Cedex, France

C. RICHARD, J. P. PILLOT, J. DUNOGUES
Laboratoire de Chimie Organique et Organométallique (URA-35 CNRS), Université Bordeaux I, 351 Cours de la Libération, F-33405, Talence, France

C. GERARDIN, F. TAULELLE
Laboratoire des Materiaux Inorganique, Université Paris VI, 4–6 Place Jussieu, F-75252, Paris Cedex 05, France

Novel polycarbosilazanes (PCSZs) were prepared by stepwise synthesis and thermal cross-linking of polysilasilazane (PSSZ) copolymers. Their pyrolysis under inert gas, producing Si–C–N ceramics, was investigated up to 1600 °C by analyses performed on the solids (elemental analysis; EPMA; TGA, density; ^{1}H, ^{13}C and ^{29}Si solid state NMR, i.r. XRD, electrical conductivity) and analyses of the evolved gases (gas chromatography and mass spectrometry). From 250 to 450 °C, a first strong weight loss was observed, which was due to the formation and elimination of low-boiling-point oligomers. The weight loss closely depends on the cross-linking degree of the ceramic precursor resulting from the PSSZ/PCSZ conversion. Then, the organic/inorganic transition took place between 500 and 800 °C, proceeding via evolution of gases (mainly H_2 and CH_4) and yielding a hydrogenated silicon carbonitride. This residue remained stable up to 1250 °C although it progressively lost its residual hydrogen as the temperature was raised. Then, crystallization occurred between 1250 and 1400 °C, yielding β-SiC crystals surrounded by free-carbon cage-like structures. Finally, above 1400 °C, the remaining amorphous Si–C–N matrix underwent a decomposition process accompanied by nitrogen evolution and a second substantial weight loss. At 1600 °C, the pyrolytic residue was a mixture of β-SiC and free carbon. So, the amorphous silicon carbonitride resulting from the pyrolysis of PCSZ precursors was found to be appreciably more thermally stable than the previously reported Si–C–O ceramic obtained by pyrolysis of polycarbosilane precursors.

1. Introduction

Non-oxide ceramics, such as SiC and Si_3N_4, have been produced from powders by sintering for many years; this is a process which involves a high-temperature step and very often the use of sintering aids and/or high pressure [1]. This process is no longer applicable in a variety of advanced fields including electronic-device packaging and ceramic-matrix composites (CMCs). An alternative approach is to start from gaseous or liquid precursors (e.g. CH_3SiCl_3 or polycarbosilanes (PCSs) for SiC) in which the atoms that will constitute the ceramics are already bonded to each other at the molecular level and which can easily be converted into ceramics. This approach has been applied successfully to carbon [2, 3] and a variety of refractory materials e.g. SiC, Si_3N_4, B_4C, BN and AlN [4–10]. This method offers two important advantages: (i) it is highly versatile and (ii) it only requires moderate temperatures. As an example, liquid polymeric precursors have been used to produce protective films [11], ceramic fibres [12] and to a lesser extent ceramic matrices for CMCs [13, 14].

One of the most often achieved applications of the liquid-precursor route to ceramics is that which was followed by Yajima and his co-workers [15] when they prepared the first available SiC-based ceramic fibres (Nicalon fibres produced by Nippon Carbon) from a PCS-liquid precursor. The green fibre was spun from molten PCS at a temperature of about 350 °C, made infusible by oxygen curing and pyrolysed at a temperature of about 1200 °C under an inert atmosphere. Ex-PCS fibres have a high tensile strength at room

0022–2461

temperature (σ^R = 2800 MPa) due to their amorphous or poorly crystalline state and a medium stiffness (E = 200 GPa). The main drawback of ex-PCS fibres is their relatively low thermal stability; a decomposition process takes place beyond 1100 °C, with an evolution of gases, a crystallization of the residue and a drop in the failure strength. It is generally accepted that these phenomena are closely related to the oxygen content of the fibres. Many attempts made to improve the properties of such fibres have been mainly performed in two directions: (i) lowering the oxygen content (i.e. using radio- or photochemically induced curing instead of oxygen curing) [16], and (ii) by trying to shift the decomposition-temperature threshold towards higher temperatures (e.g. using polycarbosilazane (PCSZ) precursors instead of PCS precursors) [17–21].

The aim of the present contribution is to report and discuss the results of a study of the organic/mineral transition which takes place in novel polymeric precursors of Si–C–N ceramics when they are progressively heated at high temperatures under an inert atmosphere. The starting materials are PCSZs prepared by a two-step route involving the Würtz-type co-condensation of equimolecular amounts of Me_2SiCl_2 and $(MeSiHCl)_2NH$, leading to a PSSZ copolymer in good yield. To improve the char yield while retaining other interesting properties such as spinnability, the presence of thermally or chemically reactive sites (i.e. Si–H, N–H and Si–Si bonds) enables controlled cross-linking to be performed. Accordingly, to investigate the influence of the precursors's structure upon the ceramic properties, three PCSZs corresponding to different degrees of PSSZ/PCSZ conversion were prepared.

These PCSZs are members of a novel family of precursors in which the nitrogen content can be continuously modified by simply changing the proportions of the monomers [22, 23]. These precursors have advantages, when properly cross-linked, which include: (i) melting without any appreciable decomposition (up to 350 °C), (ii) solubility in several common organic solvents, and (iii) rheological properties in the molten state which are well suited to dry spinning.

2. Experimental procedure

2.1. Synthesis of the ceramic precursors

First, dimethyldichlorosilane (0.1935 kg, 1.5 mol) and 1,3-dichloro-1,3-dimethyldisilazane (0.2615 kg, 1.5 mol) [23] were added dropwise under argon to a vigorously stirred suspension of sodium (0.145 kg, 6.3 mol) in boiling toluene (1200 ml) over a period of 5 h. At the end of the addition, the reaction mixture was kept under reflux for 24 h and then allowed to cool to room temperature, resulting in the precipitation of a substantial amount of insoluble materials (sodium chloride and residual sodium). Then the mixture was filtered off under inert gas and the solid washed twice with pentane or ether (2 × 400 ml). The combined organic layers were concentrated under reduced pressure with a rotary evaporator to remove a substantial amount of solvent. Anhydrous gaseous ammonia was then bubbled at 0 °C to eliminate the remaining Si–Cl bonds. The ammonium-hydrochloride precipitate was filtered off under argon and the solvent removed by distillation with a rotary evaporator. Careful devolatilization under high vacuum ((13, 3 Pa), 150 °C, 3 h) allowed the removal of any trace of solvent and a small amount of low-boiling-point oligomers yielding a clear mobile PSSZ copolymer (0.173 kg, 71.6% yield, $\bar{M}_w$ = 2500; I_p = 2.1). Its char yield was only 21.1% (thermogravimetric analysis (TGA), 950 °C under argon flow), showing that its structure is poorly cross-linked as expected (Fig. 1).

In the second step, PSSZ was progressively heated in a three-necked quartz vessel equipped with a reflux condenser and an inert-gas inlet. When the mixture temperature reached 250–270 °C, regular gas evolution occurred and oligomers condensed in the flask. The PSSZ/PCSZ conversion rate was monitored by measuring the gas evolution and by careful observation of the polymer viscosity. This conversion includes partial transformation of PSSZ into PCSZ with simultaneous formation of volatile oligomers and thermal cross-linking condensation reactions. As soon as the expected volume of gas and the desired viscosity were reached, the PCSZ was allowed to cool at room temperature under argon. Hexane was then added and the mixture magnetically stirred for a few hours. The solution was filtered under argon to remove any trace of insoluble material and the solvent distilled under vacuum (13, 3 Pa). After removing a small fraction of volatile oligomers, a yellowish, solid PCSZ was obtained (at this stage of the procedure, the following standard devolatilization conditions were used for all the PCSZ: 0.1 torr (13, 3 Pa), 250 °C, 3 h).

Thus, PCSZ-I was prepared in 77.5% yield (maximum thermolysis temperature, 335 °C). PCSZ-II was obtained in 86% yield by heating an aliquot fraction of PCSZ-I under similar conditions but up to a higher temperature (maximum thermolysis temperature, 372 °C). PCSZ-III was prepared in 76.6% yield as an insoluble and unmeltable solid, by thermal treatment of PSSZ in an autoclave (470 °C, 22 h, final pressure, 7.2 MPa).

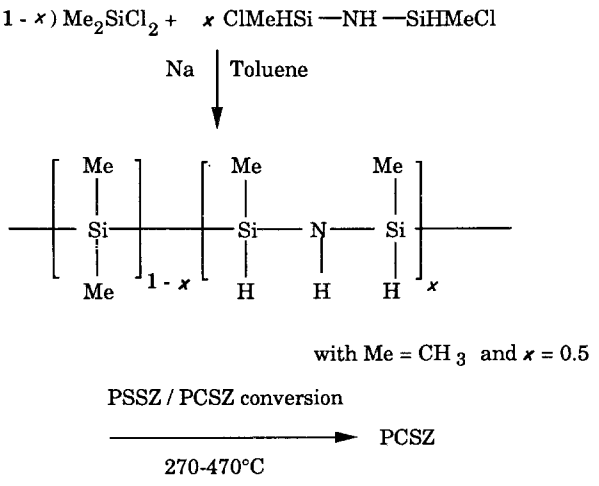

Figure 1 Synthesis of PSSZ and PCSZ copolymers.

2.2. Pyrolysis conditions

For $\theta_p < 850\,^{\circ}C$ (θ_p being the highest temperature reached during pyrolysis), a PCSZ sample was put in an alumina boat and heated in a glass silica tube under a high-purity argon flow (flow rate; $1\,l\,h^{-1}$ of argon N56 grade from Air Liquide) under a pressure of 100 kPa. The temperature was progressively raised up to θ_p (at a rate of $5\,^{\circ}C\,min^{-1}$) and kept at this value for 1 h.

For $\theta_p > 850\,^{\circ}C$, the sample (pre-pyrolysed at 850 °C as above) was put in a graphite crucible, heated rapidly ($60\,^{\circ}C\,min^{-1}$) at θ_p under a high-purity argon flow at a pressure of 100 kPa with a radio frequency coil and kept at this temperature for 1 h (or 6 h for few samples).

2.3. Characterization techniques

Elemental analyses were performed by two different procedures: (i) by conventional bulk chemical analysis (CNRS, Service Central d'analyse, BP 22 F-69390 VERNAISON) on both the organic and mineral samples [20] and (ii) by electron probe microanalysis (EPMA, CAMEBAX 75 from CAMECA) in the wavelength-dispersion mode (PET crystal for SiK_α and a multilayer PCI for CK_α; NK_α and OK_α) with standards (SiC, SiO_2, $Si_xN_yO_z$ and BN) whose compositions were either assumed to be stoichiometric (single crystals) or already known. The hydrogen content of the samples was assessed by proton nuclear magnetic resonance (NMR) spectroscopy [25].

The density of the samples was measured by the floating technique in liquid mixtures (dibromohexane/bromoform or dibromohexane/hexane) maintained at a constant temperature, whose density was progressively varied by changing their composition.

Thermogravimetric analyses (TGAs) were performed, up to 950 °C, in platinum crucibles on 1–5 $\times 10^{-5}$ kg samples under a flow of pure argon (flow rate $1\,l\,h^{-1}$) with a rate of temperature increase of $5\,^{\circ}C\,min^{-1}$. Beyond 950 °C they were performed in a graphite crucible/furnace under a flow of pure helium (N 56 grade from Air Liquide) and with a rate of temperature increase of $10\,^{\circ}C\,min^{-1}$.

The infrared (i.r.) spectra were recorded in the transmission mode in the 400–4000 cm^{-1} range, in the following ways: (i) from neat films between KBr plates for the PCSZ precursors (Perkin Elmer 1420 or 683 spectrometers), and (ii) from pressed pellets made from a mixture of KBr powder and the finely ground samples, for the pyrolytic residues.

The gases formed during the pyrolysis of the precursors were analysed by two different procedures depending on the value of θ_p.

1. For $\theta_p < 1000\,^{\circ}C$, the sample (a few grammes) was set in a furnace and progressively heated at $1\,^{\circ}C\,min^{-1}$ up to 400 °C then at $1–5\,^{\circ}C\,min^{-1}$ up to θ_p under a flow of pure nitrogen (N 56 grade from Air Liquide, flow rate, $1\,l\,h^{-1}$, at atmospheric pressure). Ammonia formed during pyrolysis was measured by acidimetry, whereas the other gaseous components were analysed by chromatography. The flow rates of the various gaseous species were determined with respect to the flow of nitrogen. The compound species which condensed on the wall of the furnace were identified by elemental analysis and i.r. spectrometry.

2. For $\theta_p > 1200\,^{\circ}C$, the samples (pre-pyrolysed at 1000 °C as above) were put in a microfurnace connected to a high-resolution mass spectrometer (VG 7070 F mass spectrometer) by a capillary tube of suitable size, to qualitatively assess the nature of the gaseous components.

Gel permeation chromatography (GPC) was used to determine average molecular weights, using five μ-styragel columns (porosity ranges of 10, 50, 10^2, 10^3 and 10^4 nm) and THF as the eluent at a flow rate of $1\,ml\,min^{-1}$. Molecular weights were obtained from polystyrene standards (eleven points calibration curve, the detection system being a Wasters Associates Differential Refractometer R401).

The NMR spectra were recorded from both the organic and mineral materials, either in solution (with C_6D_6 as the solvent) or in the solid state. Three different NMR spectrometers were used: a Brucker AC250 spectrometer for ^{13}C and ^{1}H (at resonance frequencies of 250.13 MHz and 62.9 MHz, respectively) and a Brucker AC200 or a MSL400 spectrometer for ^{29}Si (at a resonance frequency of 79.5 MHz, magic-angle rotation). The procedures have been described elsewhere in a detailed manner [26].

The X-ray diffraction (XRD) spectra (CuK_α, Philipps PW-1710 diffractometer control) were recorded from finely ground samples. The apparent mean grain size (L) of the β-SiC crystalline phase present in some of the samples (as discussed below) was calculated from the width (D) of the (1 1 1) diffraction peak at mid-height, according to the following equation:

$$L = K\lambda/D\cos\theta \quad (1)$$

where K is a constant (taken as 1), λ the CuK_α wavelength (i.e. $\lambda = 0.154$ nm) and θ the Bragg angle ($\theta = 17.8°$ for β-SiC (1 1 1)).

The electrical conductivity of the pyrolytic residues was measured on fragments of the samples, by the four-point method, from room temperature to 600 °C (both on heating and cooling) under an atmosphere of pure helium. The data (plotted as a $\ln\sigma = f(1/T)$ graph, σ being the electrical conductivity and $1/T$ the reciprocal temperature) were used to assess the apparent activation energy when the samples exhibited a semiconducting behaviour.

Finally, the change in morphology occurring in the samples during the pyrolysis was studied by scanning electron microscopy (SEM) (JEOL 840 S).

3. Results

3.1. Nature of the PCSZ precursors

Softening temperatures (measured on a KOFLER hotbench) and the average mass molecular weights $\bar{M}_w$ measured for the three PCSZ precursors are listed in Table I. The softening temperature of the ceramic precursor closely depends on the thermolysis conditions applied to the PSSZ copolymers. Mild conditions yielded a polycarbosilazane (PCSZ-I) soluble in

hexane which exhibits a low softening temperature. Severe thermolysis conditions yielded an insoluble and unmeltable polymer (PCSZ-III). Interestingly, intermediate degrees of PSSZ/PCSZ conversion could be easily achieved either by careful monitoring of the step 2 thermal-treatment conditions or by performing two successive treatments (PCSZ-II). Thus, it has been established that it was possible to increase the softening temperature of the precursor while retaining a good solubility. Furthermore, Table I clearly shows that the average mass molecular weight $\bar{M}_w$ also depends closely on the thermolysis treatment (the more intense the cross-linking, the higher the values of both $\bar{M}_w$ and I_p).

3.1.1. Elemental analysis

Results of the elemental analyses of PCSZ-I–III are given in Table II. The measured values for silicon are consistent with those calculated from the theoretical formula of the initial PSSZ copolymer (Fig. 1). The values measured for nitrogen are slightly higher than the calculated ones; a feature which might be related to the ammonia treatment used to eliminate the remaining Si–Cl bonds at the first step. On the other hand, both the carbon and hydrogen percentages measured are slightly lower than those expected (the discrepancy could simply be assigned to a lack of accuracy and reliability of bulk-elemental conventional analysis when applied to such materials). Finally, it is worthy of note that the total amount of oxygen in the precursor is fairly low (i.e. of the order of 1.5% for the precursors submitted to a single thermolysis treatment, and of the order of 3% when two thermolyses were successively carried out).

3.1.2. Structure

Owing to the well-known methylene-group insertion into Si–Si bonds [27], Si–CH_2–Si–N units are expected to be formed in the main skeleton of the preceramic polymers, either during the thermolysis (step 2) of the processing procedure or at a very early stage of the following pyrolysis itself. Indeed, such units could be expected to foreshadow, to a certain extent, part of the framework of the final silicon carbonitride-based ceramics. It is worth noting that such an ability did not exist for the polysilazanes (PSZ) that were previously used for the preparation of Si–C–N ceramics with the exception of the precursors obtained from chlorinated disilanes [28].

The above assumptions are supported by the i.r. spectroscopy data since characteristic absorptions of Si–CH_2–Si groups at 1350 and 1040 cm^{-1} were observed, closely depending on the degree of PSSZ/PCSZ conversion (Fig. 2); these bands are not observed for PCSZ-I but they are already present for PCSZ-II. Moreover, a considerable decrease of the N–H absorption (at 3380 cm^{-1}) also occurs showing that nitrogen atoms undergo trisilylation to a large extent.

PSSZ and PCSZ-II ^{29}Si NMR spectra (Fig. 3) are somewhat complex, showing considerable broadening of signals for the PCSZ-II precursor. In the case of the PSSZ copolymer, it is noteworthy that, for $x = 0.5$, (see Fig. 1), only a very small proportion of polydimethylsilane structural units, i.e. Si–$\underline{Si}Me_2$–Si units, are formed as only a very weak multiplet in the − 40 p.p.m. region is observed (Fig. 3). On the basis of INEPT experiments, the main multiplet, centred at − 22 p.p.m., is assigned to N–$\underline{Si}$MeH–Si and N–$\underline{Si}$MeH–N nuclei. The signals in the range − 12 to 0 p.p.m. are assigned to N–$\underline{Si}Me_2$–Si and N–$\underline{Si}Me_2$–N nuclei. Similarly, the ^{29}Si NMR spectrum of PCSZ-I reveals the decrease of the

TABLE I Some properties of PCSZ-I–III Si–C–N ceramic precursors, I_p: polydispersity

PCSZ precursors	$\bar{M}_w$	I_p	Softening temperature (°C)
PCSZ-I	5270	2.8	90–100
PCSZ-II	15250	7.5	170
PCSZ-III	–	–	> 250

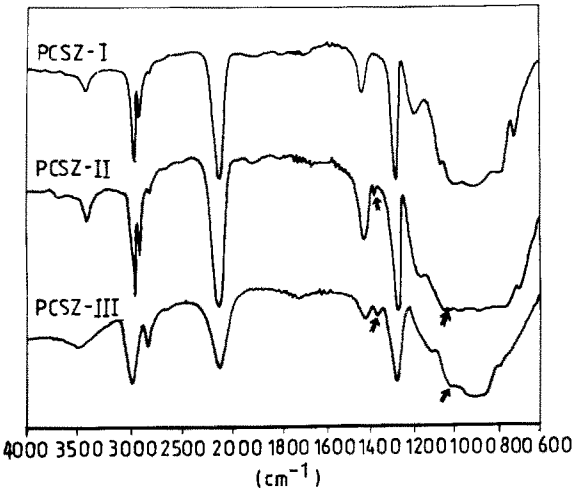

Figure 2 I.r. spectra of the PCSZ precursors.

TABLE II Bulk elemental calculated (calc.) or found compositions of the PCSZ precursors

PCSZ	Si (wt %)		C (wt %)		N (wt %)		H (wt %)		O (wt %)	
reference	Calc.	Found	Calc.	Found	Calc.	Found	Calc.	Found	Calc.	Found
PCSZ-I	52.2	52.9	29.8	26.8	8.7	11.7	9.3	7.7	–	1.4
PCSZ-II	52.2	52.5	29.8	25.4	8.7	12.2	9.3	6.9	–	2.9
PCSZ-III	52.2	52.9	29.8	26.4	8.7	12.2	9.3	6.5	–	1.4

N–$\underline{Si}Me_2$–Si multiplet intensity and the enhancement of the broad signal centred at − 22 p.p.m. Thus, we can assume that this multiplet includes N–SiMeH–CH_2–Si units as well as residual N–SiMeH–Si and N–SiMeH–N units. The fact that PSZ units presumably occur confirms that an appreciable proportion of N–H bonds undergo trisilylation during the overall process. Part of these units might also arise from the substitution of the chlorinated-chain-ends by nitrogen during the final treatment with gaseous ammonia (i.e. N–$\underline{Si}$MeH–Cl and N–$\underline{Si}Me_2$–Cl terminals).

More details about the physico-chemical characterization of these ceramic precursors will be provided in a forthcoming paper [29].

3.2. Pyrolysis of the PCSZ precursors

3.2.1. TGA

When PCSZ-I–III are heated under an inert atmosphere of pure argon at increasing temperatures, θ_p, different weight losses occur as shown in Fig. 4.

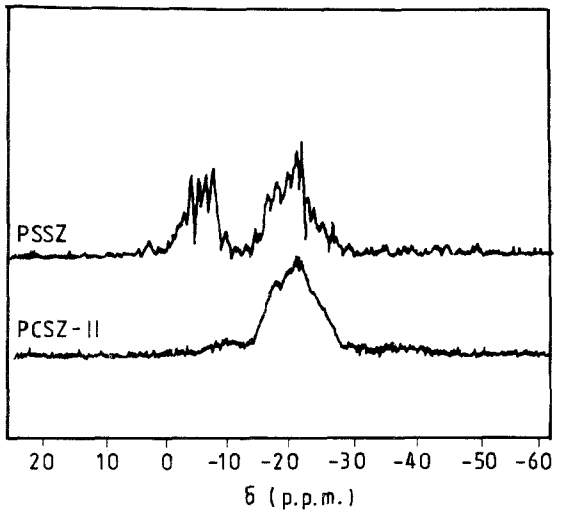

Figure 3 Solution ^{29}Si NMR spectra of PSSZ and PCSZ-I (INEPT).

Within the temperature range 25–950 °C, a first weight loss occurs as θ_p is increased, followed by a plateau in the TGA curve for $\theta_p > \theta_2$ (Fig. 4a). For PCSZ-I and PCSZ-II, the weight loss starts early, i.e. at about 200 °C, and is large and very rapid up to θ_1 = 450 °C whereas for PCSZ-III it is still undetectable at θ_1 = 450 °C. Furthermore, for $\theta_1 < \theta_p < \theta_2$, the weight loss slows for PCSZ-I and PCSZ-II whereas the major part of the overall weight loss for PCSZ-III occurs in this temperature range. Finally, the θ_2 value regularly increases from precursor I to precursor III in the PCSZ-series. It thus appears that, within the temperature range 25–950 °C, there is a clear correlation between the main features of the TGA curve and the degree of the PSSZ/PCSZ conversion of the material. When this degree of conversion is low (e.g. in PCSZ-I), the weight loss is very large and starts at a low temperature. On the contrary, when it is high (PCSZ-III), the weight loss is much smaller and shifted towards higher temperatures.

As shown in Fig. 4b, a second weight loss occurs when the materials, pre-pyrolysed at 850 °C, are further heated under an inert atmosphere within the temperature range 25–1600 °C. This second weight loss starts at about 1250 °C which means that the plateau observed beyond θ_2 in the TGA curves shown in Fig. 4a extends up to 1250 °C, whatever the nature of the PCSZ sample. However, the value of the second weight loss at 1600 °C is higher for PCSZ-III (i.e. 28%) than for PCSZ-I (21%).

3.2.2. Elemental composition of the pyrolytic residues

The results of the elemental chemical analyses performed on the pyrolytic residues are shown in Tables IIIa,b and IV for PCSZ-I and PCSZ-III. Although there may be some uncertainty in the data, related to analytical difficulties (e.g. that of an accurate analysis of hydrogen in low mass samples), it clearly appears that the two successive weight losses observed by TGA are related to changes in the solid-residue composition. The first, occurring below 850 °C, is related to a dramatic decrease in the hydrogen content of the

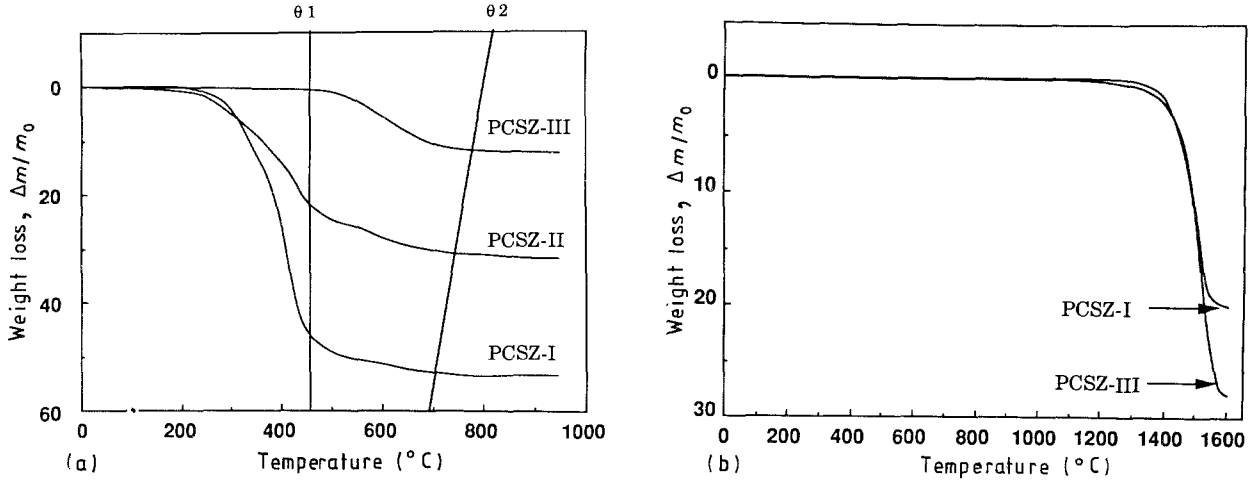

Figure 4 TGA curves for the three precursors showing the weight loss ($\Delta m/m_0$) and pyrolysis yield (m/m_0) as a function of θ_p within the temperature ranges: (a) 25–950 °C and (b) 25–1600 °C for materials prepyrolysed at 850 °C.

TABLE III Elemental analyses of the pyrolytic residues of PCSZ-I for different θ_p values, obtained by EPMA unless specified otherwise (* data from bulk conventional chemical analysis, ** estimated from gas analysis, *** derived from ^{1}H NMR spectra). (a) Hydogen not taken into account and (b) hydrogen taken into account

(a)

θ_p (°C)	Elemental analysis (at % (wt %))			
	Si	C	N	O
850	43 (62.1)	34 (21.0)	21 (15.2)	2 (1.7)
950	43 (62.1)	34 (21.0)	21 (15.2)	2 (1.7)
1100	43.5 (62.4)	34 (20.9)	21 (15.1)	2 (1.7)
1400	43.5 (62.4)	32.5 (20.3)	20 (14.6)	2 (1.7)
1600	43 (63.6)	50 (31.7)	3 (2.2)	3 (2.5)

(b)

θ_p (°C)	Elemental analysis (at %)				
	Si	C	N	H	O
25	14*	17.5*	7*	61*	0.4*
850	31	26.8	15.5	25.7**	0.9
950	38	30	18.5	12**	1.8
1100	40.5	31.7	19.6	7.4**	1.9
1400	43.5	32.5	20	< 0.2***	2
1600	43	50	3	< 0.1***	3

TABLE IV Elemental analysis of the pyrolytic residues of PCSZ-II for increasing values of θ_p; results obtained by EPMA, hydrogen not taken into account

θ_p (°C)	Elemental analysis (at % (wt %))			
	Si	C	N	O
850	45 (64.3)	31 (19)	20 (14.3)	3 (2.4)
950	44 (63)	33 (20.2)	20 (14.3)	3 (2.5)
1100	44 (63)	33 (20.2)	20 (14.3)	3 (2.5)
1400	44 (63)	33 (20.2)	20 (14.3)	3 (2.5)
1600	44 (64.2)	50 (31.8)	2 (1.5)	3 (2.5)

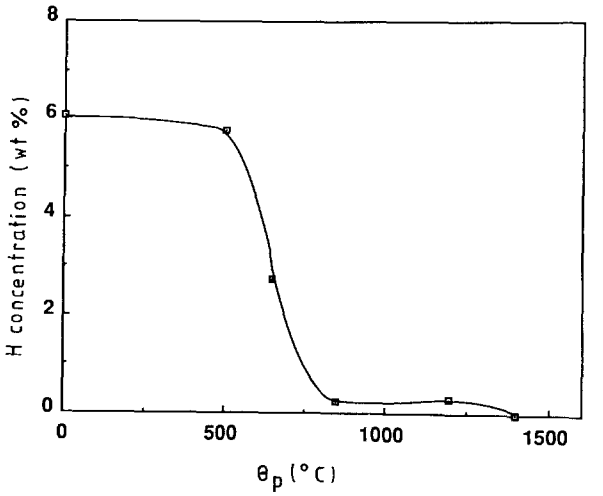

Figure 5 Variations of the hydrogen content of the pyrolytic residue of PCSZ-II, as measured by ^{1}H NMR, versus the pyrolysis temperature θ_p.

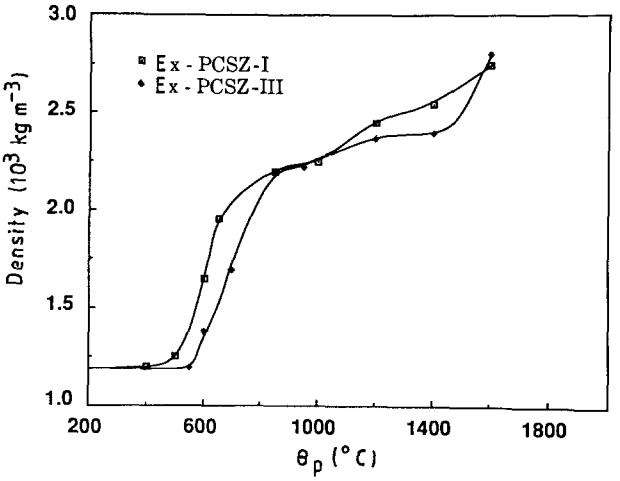

Figure 6 Density variation of the PCSZ-I and PCSZ-III pyrolytic residues as a function of the pyrolysis temperature.

residue, as shown in Fig. 5. The second, above 1400 °C, results in a large drop in the nitrogen concentration (i.e. from 20 to 3 at % when θ_p is raised from 1400 to 1600 °C for PCSZ-I). Furthermore, it is worth noting that: (i) the hydrogen content of the pyrolytic residue remains quite significant at rather high temperatures (e.g. it is still 7.4 at % at 1100 °C for PCSZ-I); (ii) the final residue, obtained for $\theta_p = 1600$ °C, is likely to contain free carbon (based on the assumption that silicon is bonded to carbon as SiC); (iii) some evolution of silicon might occur along with that of nitrogen at $1400 < \theta_p < 1600$ °C (since the Si/C ratio falls from 1.34 for $\theta_p = 1400$ °C to 0.86 for $\theta_p = 1600$ °C); and finally (iv) the oxygen contamination of the pyrolytic residue is low (i.e. 1–2 at % for $850 < \theta_p < 1400$ °C) despite the well-known sensitivity of PCSZ to oxygen and moisture.

3.2.3. Density

The variations of the pyrolytic-residue density as a function of θ_p are shown in Fig. 6, for PCSZ-I and PCSZ-III. For each material, there is first a sharp increase in density at low θ_p (taking place between 400–700 °C for PCSZ-I and between 500–850 °C for PCSZ-III) followed by a much slower increase in density from 850 to 1600 °C. Although the sharp transition takes place earlier for PCSZ-I, the final densities for the two pyrolytic residues are the same, i.e. about 2.75×10^3 kg m^{-3} for $\theta_p = 1600$ °C.

3.2.4. I.r. spectrometry analysis

The i.r. spectra of the pyrolytic residues of PCSZ-I and PCSZ-III are shown in Fig. 7 for increasing θ_p values and the observed absorption bands are listed in Table V.

3.2.4.1. For $\theta_p < 450$–500 °C. There are only minor changes in the i.r. spectra, the main absorption bands are still those of the initial organosilicon polymers. However, for PCSZ-I (i.e. that corresponding to a low degree of PSSZ/PCSZ conversion) several changes are

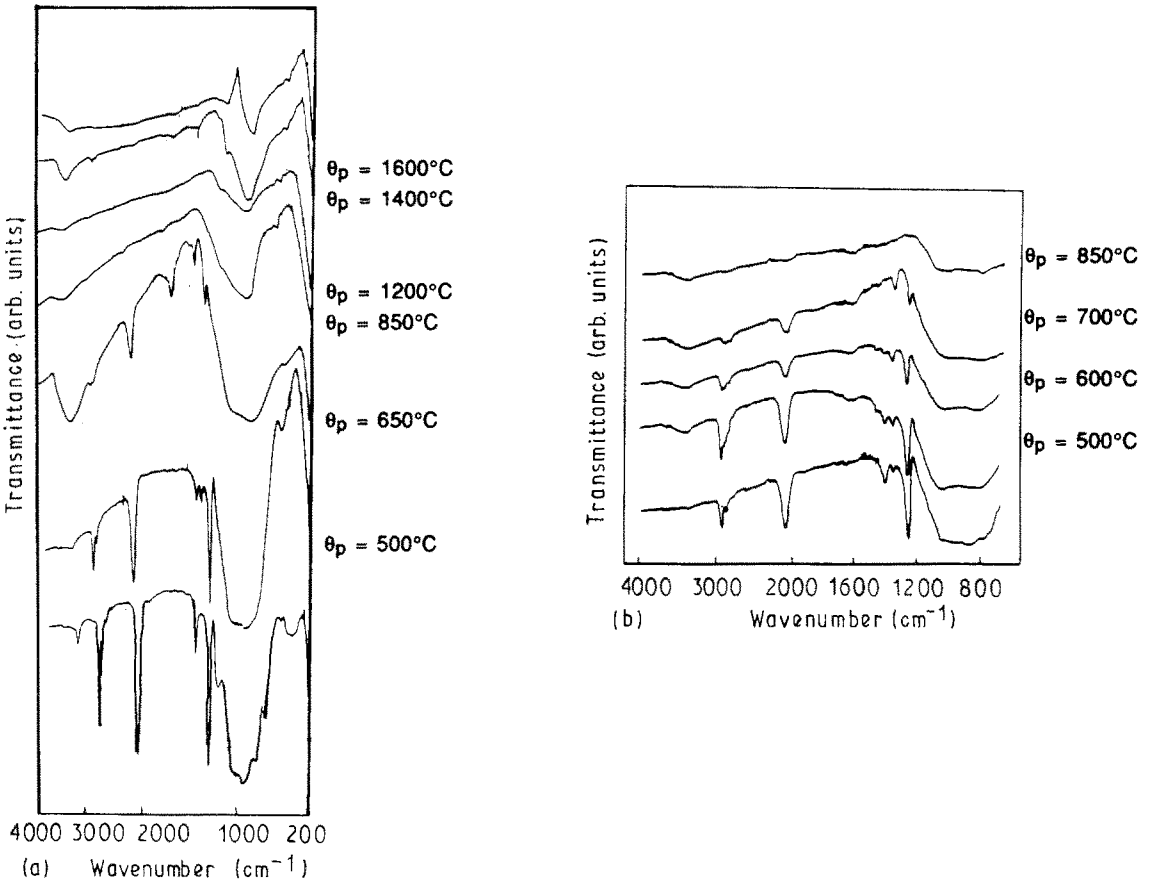

Figure 7 I.r. spectra of PCSZ precursors and of their pyrolytic residues at increasing pyrolysis temperatures: (a) PCSZ-I, and (b) PCSZ-III.

actually observed when θ_p is raised from room temperature to 500 °C: (i) the absorption bands at 3450 and 1160 cm^{-1}, assigned to a valence vibration ν(N–H) and a deformation γ(N–H), disappear; (ii) the very strong absorption band at 2130 cm^{-1}, assigned to ν(Si–H), decreases in intensity; (iii) the weak absorption band at 400 cm^{-1} assigned to Si–Si, vanishes; and finally (iv) a weak absorption band at 1350 cm^{-1}, assigned to ω(Si–CH_2–Si) appears. As discussed in Section 4.1.1, these changes in the i.r. spectra support the occurrence of a PSSZ/PCSZ conversion taking place in the material by insertion of a methylene group into the Si–Si bonds (according to a mechanism previously described by Shiina and Kumada [30]). This result is consistent with the difference between PCSZ-I and PCSZ-III, mentioned in Section 3.1.

3.2.4.2. For 500 < θ_p < 850 °C. The i.r spectra of the pyrolytic residues exhibit strong changes. On the one hand, at 650 °C, the ratio between the intensity of the ω(Si–CH_2–Si) absorption band at 1350 cm^{-1} and that of the ν(Si–CH_3) absorption band at 1400 cm^{-1} has still increased with respect to its value at 500 °C, for PCSZ-I. This feature suggests that the PSSZ/PCSZ conversion continues to proceed, at least near the lower side of the temperature range. On the other hand, when θ_p is raised from 500 to 850 °C, the intensities of the ν(Si–H), ν(C–H) and ω(Si–CH_2–Si) absorption bands undergo a dramatic decrease: they almost disappear at 850 °C, which clearly shows that a new transformation, referred to as the organic/inorganic transition, takes place within this temperature range and that it can be considered as almost achieved at 850 °C.

3.2.4.3. For 850 < θ_p < 1600 °C. There is little change in the i.r. spectra of the pyrolytic residues with the exception of: (i) a remaining absorption band at 2900 cm^{-1} (assigned to ν(C–H)) which suggests that some hydrogen is still bonded to carbon, at least for the lower side of the temperature range (in agreement with the elemental chemical analysis); and (ii) some sharpening of the broad absorption bands at 850 and 1100 cm^{-1}, for θ_p > 1400 °C which could be assigned to silicon carbide [31].

3.2.5. Gas analysis

Analysis of the gases formed during the pyrolysis of PCSZ-I and PCSZ-III was performed in the two temperature ranges (i.e. 25–1000 °C and 1200–1700 °C) corresponding to the weight losses observed by TGA and to the changes in the chemical composition of the pyrolytic residue (Figs 8 and 9a–b, and Tables VI and VII).

3.2.5.1. 25 < θ_p < 1000 °C. At low temperatures, i.e. for θ_p < 450 °C, the behaviours of PCSZ-I and PCSZ-III are very different, as expected from the respective

TABLE V Main absorption bands observed in the i.r. spectra of PCSZ precursors and pyrolytic residues vs: very strong; s: strong; m: medium; w: weak

Wave number (cm^{-1})	Intensity	Assignment	Wave number (cm^{-1})	Intensity	Assignment
3450	m	ν(N–H)	1260	s	δ(Si–CH_3)
2960	s	ν(C–H)	1160	m	γ(N–H) (Si–NH–Si)
2890	m	ν(C–H)	1045	m	δ(Si–CH_2–Si)
2800	w	ν(C–H)	1000–940	s (broad)	ν(Si–N–Si)
2130	vs	ν(Si–H)	940–850	vs (broad)	δ(Si–H)
1410	m	δ(C–H) (CH_3)	830	s	ρ(CH_3–Si)
1350	w	ω(Si–CH_2–Si)	400	w	ν(Si–Si)

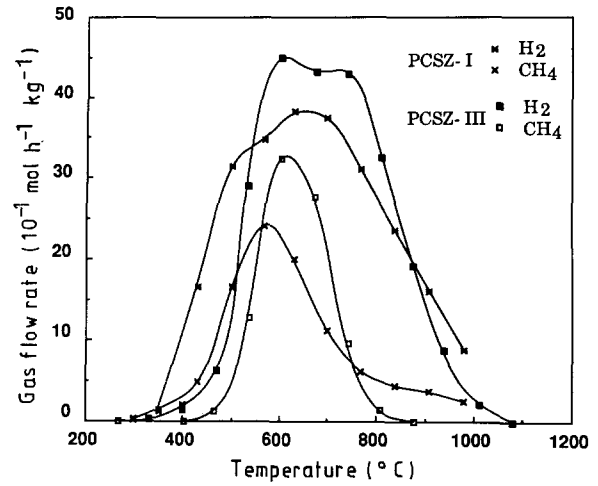

Figure 8 Variation of the hydrogen and methane gas-flow rates (measured by gas chromatography) as a function of temperature, during the organic/inorganic transition of PCSZ (the gas flow rate data are given per kg of residue at 450 °C).

TABLE VI Analysis of the gaseous hydrocarbon species (by gas chromatography) formed during the pyrolysis of PCSZ-I at increasing temperature; Q is the gas flow rate

θ_p (°C)	Q ($\times 10^{-1}$ mol h^{-1} kg^{-1})			
	H_2	CH_4	C_3H_6	C_4H_8
300	0.15	0.1	0.07	–
350	0.75	0.7	0.3	0.4
400	1.19	0.9	0.6	0.8
430	9.11	2.7	0.2	0.3
500	17.35	9.15	0.1	1
570	19.24	13.3	0.09	1.1
630	21.1	11.0	0.04	1.0
700	20.7	6.2	0.04	1.0
770	17.2	3.4	–	0.2
840	13.0	2.4	–	0.1
910	8.9	2.1	–	0.3
980	4.9	1.4	–	0.4

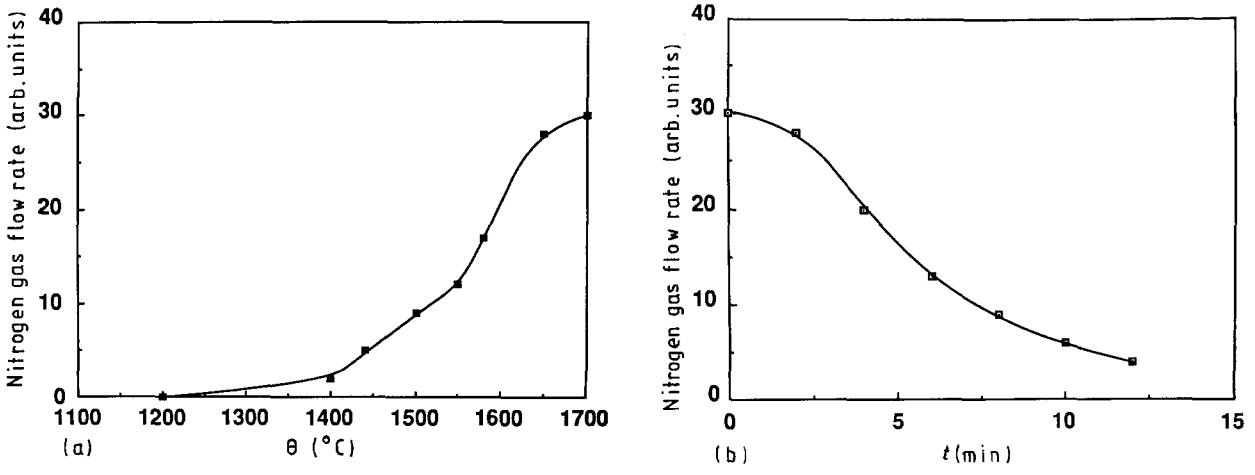

Figure 9 Variations of nitrogen gas flow rate during the pyrolysis of PCSZ-II as a function of: (a) temperature, and (b) time at 1700 °C.

PSSZ/PCSZ degrees of conversion of both precursors. For PCSZ-I, two types of low-volatility products are condensed on the cold wall of the pyrolysis apparatus, for $150 < \theta_p < 450$ °C: (i) an oil whose i.r. spectrum is very similar to that of PCSZ-I, and (ii) a small amount of solid whose i.r. spectrum exhibits a weak absorption band at 1050 cm^{-1} assigned, to Si–O bonds. The corresponding weight loss is of the order of 45%, as shown in Fig. 4. Whereas the same treatment of PCSZ-III yields no condensable volatile products and the weight loss is negligible.

Beyond 450 °C, both methane and hydrogen are evolved in large amounts as well as traces of butene and propylene, for all the PCSZ-precursors, as shown in Fig. 8 and Table VI. The overall amount of gas formed between 450 and 1000 °C is lower for PCSZ-I than for PCSZ-III, since 45% of the mass of PCSZ-I is lost by volatilization below 450 °C as mentioned

above. To take into account this important phenomenon, the flow rates of the gas formed during the pyrolysis of PCSZ are expressed in Fig. 8 per unit mass of pyrolytic residue remaining in the apparatus at 450 °C (and not per unit of mass of the initial sample).

As shown in Fig. 8, the curves corresponding to the evolution of CH_4 and H_2 during the pyrolysis of PCSZ-III are slightly shifted towards the high temperatures, with respect to those observed for PCSZ-I; this is consistent with the higher degree of PSSZ/PCSZ conversion of PCSZ-III. Moreover, the organic/inorganic transition occurs in a wider temperature range for PCSZ-I than PCSZ-III as shown by the tails of the CH_4 and H_2 curves for PCSZ-I on the high-temperature side. However, the overall amounts of pyrolytic gas and the overall weight losses observed during the organic/inorganic transition of PCSZ-I and PCSZ-III appear to be of the same order, when they are expressed per unit of residue mass at 450 °C (Table VII).

Besides the gaseous components identified by chromatography (i.e. hydrogen, methane, propylene and butene), traces of Me_2SiH_2 and $MeSiH_3$ are also formed during the flash pyrolysis of PCSZ-I below 600 °C (on the basis of mass spectroscopy analysis). Finally, a very small amount of ammonia is formed below 400 °C, corresponding to a weight loss of 0.34 wt %. Thus it appears that the main gases formed during the organic/inorganic transition of PCSZ are hydrogen and methane. In the case of PCSZ-I this transition is preceded by a weight loss of approximately 50% due to the vaporization of low boiling point products.

3.2.5.2. 1000 < θ_p < 1700 °C. As already mentioned, there is a plateau in the weight loss versus temperature curve at medium temperatures and it is only for $\theta_p > 1300$ °C that a new significant evolution of gas, namely nitrogen, is observed (Fig. 9). The evolution of nitrogen remains slow up to 1400 °C, then it increases as the temperature is raised to 1700 °C. At the latter temperature and under a total pressure of 1 Pa, evolution of nitrogen goes to completion within about 15 min. Within the 1200–1700 °C range, CO is also formed to a very small extent (on the basis of high-resolution-mass-spectroscopy data), and this is consistent with the low oxygen concentration in the pyrolytic residues (Table IIIa) and with the results previously reported on the pyrolysis of ex-PCS fibres [32]. It is likely that some trace of SiO could be formed, but this gas, stable only at high temperatures [33], was not identified.

3.2.6. Solid-State NMR Analysis

^1H, ^{13}C and ^{29}Si NMR spectra were checked to study the variations of the short-range atomic order, in the solid state, as a function of θ_p. The NMR spectra are given in Fig. 10 for PCSZ-I.

3.2.6.1. ^1H NMR (magic-angle spinning (MAS)). The ^1H MAS-NMR spectra are given in Fig. 10a for those pyrolytic residues containing enough hydrogen; i.e. those residues obtained at relatively low temperatures (θ_p = 500 and 650 °C). The spectrum of the PCSZ-I precursor exhibits two peaks: a strong peak at 0.2 p.p.m assigned to Si–C–H protons and a much weaker peak at 4.5 p.p.m assigned to Si–H protons. When θ_p is raised from 500 to 650 °C the intensity of the first peak remains unchanged whereas that of the second decreases.

3.2.6.2. ^{13}C NMR (cross-polarization magic-angle spinning (CPMAS)). ^{13}C NMR analysis, when performed in the CPMAS mode, requires samples which still contain an appreciable proportion of protons. Thus, it has been limited to pyrolytic residues prepared at low θ_p values (i.e, $\theta_p \leq 850$ °C) (Fig. 8). As shown in Fig. 10b, the spectrum of the as-prepared PCSZ-I precursor exhibits two peaks: a strong peak at 5 p.p.m. assigned to N–Si($\underline{C}H_3$)–N and a weak peak at − 7 p.p.m. assigned to –Si($\underline{C}H_3$)$_2$–. In the spectrum of the pyrolytic residue prepared at θ_p = 500 °C, the latter peak has almost completely disappeared whereas the former begins to broaden towards the high-positive-chemical-shift side, a feature related to the formation of some Si–$\underline{C}H_2$–Si sites. For θ_p = 650 °C, the spectrum is characterized by a new broad peak which is the result of a wide distribution of site population (the overall width of the peak increases from less than 10 to 30 p.p.m. when θ_p is raised from 500 to 650 °C). The fact that the peak at 5 p.p.m. is now a simple shoulder (on the right-hand side of the main broad peak) with a lower intensity and the fact that there is an overall shift of the spectrum towards the high-field side supports the occurrence of a conversion of the CH_3 groups into CH_2 and CH groups. All these features are more apparent for θ_p = 850 °C; the peak at 5 p.p.m. has almost completely disappeared and the remaining broad peak is located at 24.5 p.p.m. a chemical-shift value which corresponds to a $\underline{C}Si_4$ site (in the β-SiC standard, the related chemical shift is at 23.7 p.p.m.). The large width of the peak recorded at θ_p = 850 °C can be explained on the basis of the following remarks: (i) the carbon nuclei which have been analysed could be $\underline{C}Si_4$ or $\underline{C}HSi_3$ or even $\underline{C}H_2Si_2$, and (ii) the $\underline{C}Si_4$ sites could have different second neighbouring coordination spheres (i.e. the first neighbouring silicon of the carbon nuclei might belong to $\underline{Si}C_4$, $\underline{Si}C_3N$ or even $\underline{Si}C_2N_2$ sites).

3.2.6.3. ^{29}Si NMR (MAS). In the solid state, the ^{29}Si NMR (MAS) spectrum of the as-prepared PCSZ-I precursor is characterized by a broad peak corresponding to a distribution of chemical shifts around − 20 p.p.m assigned to $\underline{Si}N_2CH$-type sites (Fig. 10c). It is worth noting that the occurrence of $\underline{Si}NSiMeH$, $\underline{Si}N_2MeH$, $\underline{Si}N_2Me_2$ and $\underline{Si}SiNMe_2$ sites has been already deduced from the ^{29}Si NMR spectrum of the same material, but in the liquid state (Section 3.1.).

For 500 $\leq \theta_p \leq$ 850 °C, a peak corresponding to a chemical shift of − 10 p.p.m. assigned to $\underline{Si}N_2C_2$ sites,

is observed. Its intensity increases as θ_p is raised, with respect to that of the peak at -20 p.p.m. assigned to $\underline{Si}N_2CH-$ sites. For $1200 \leq \theta_p \leq 1400\,^{\circ}C$, the remaining peak becomes sharper and it is slightly shifted towards the high-field side (from -18 p.p.m. for $\theta_p = 1200\,^{\circ}C$ to -12 p.p.m. for $\theta_p = 1400\,^{\circ}C$), a feature supporting the formation of $\underline{Si}C_4$ sites.

Finally, for $\theta_p = 1600\,^{\circ}C$, the ^{29}Si NMR (MAS) peak corresponds to a chemical shift close to that observed in the β-SiC standard. However, its width is somewhat larger, as already mentioned for the ^{13}C NMR (CPMAS) spectrum.

On the basis of a quantitative analysis of the peak recorded for $\theta_p = 1400\,^{\circ}C$, it has been established that the distribution of the Si sites in the pyrolytic residue is as follows: $\underline{Si}C_2N_2$, 42.5%; $\underline{Si}C_3N$, 32.7%, and $\underline{Si}C_4$ 24.7%.

3.2.7. Structure and microstructure

The XRD patterns of the pyrolytic residues of PCSZ-I are shown in Fig. 11a for θ_p values increasing from 1100 to 1600 °C (each sample was maintained at θ_p for 1 h as described in Section 2.2.). For $\theta_p < 1300\,^{\circ}C$, the pyrolytic residues appear to be amorphous whereas for $\theta_p < 1300\,^{\circ}C$, diffraction peaks are observed and their intensities increase as θ_p is raised. The three mains lines, corresponding to *d*-spacings equal to 0.251, 0.154 and 0.131 nm respectively, were assigned to the (1 1 1), (2 2 0) and (3 1 1) reflections of β-SiC;

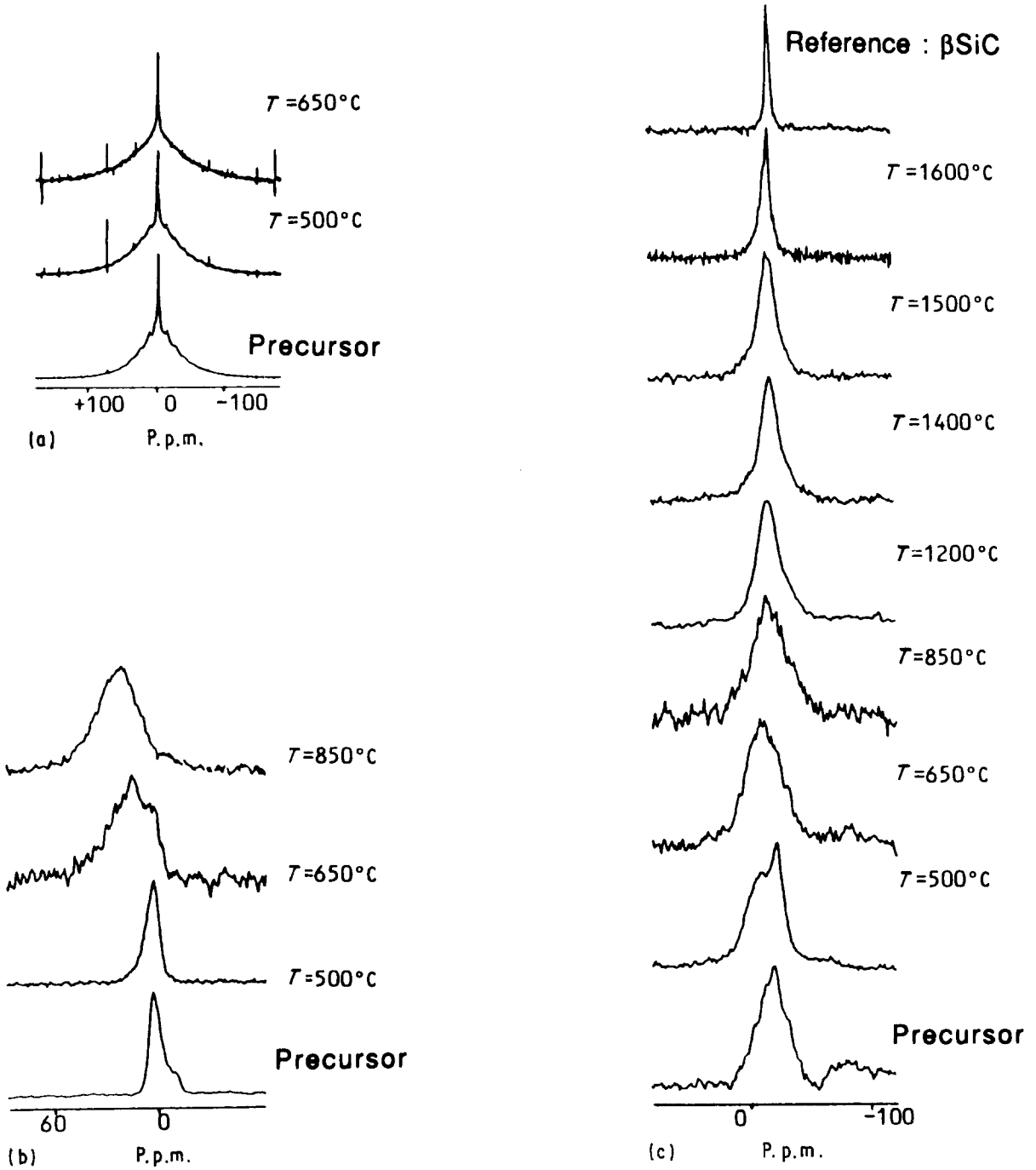

Figure 10 Solid-state NMR spectra of the as-prepared PCSZ-I precursor and its pyrolytic residues for increasing θ_p values: (a) ^1H NMR (MAS), (b) ^{13}C NMR (CPMAS), and (c) ^{29}Si NMR (MAS).

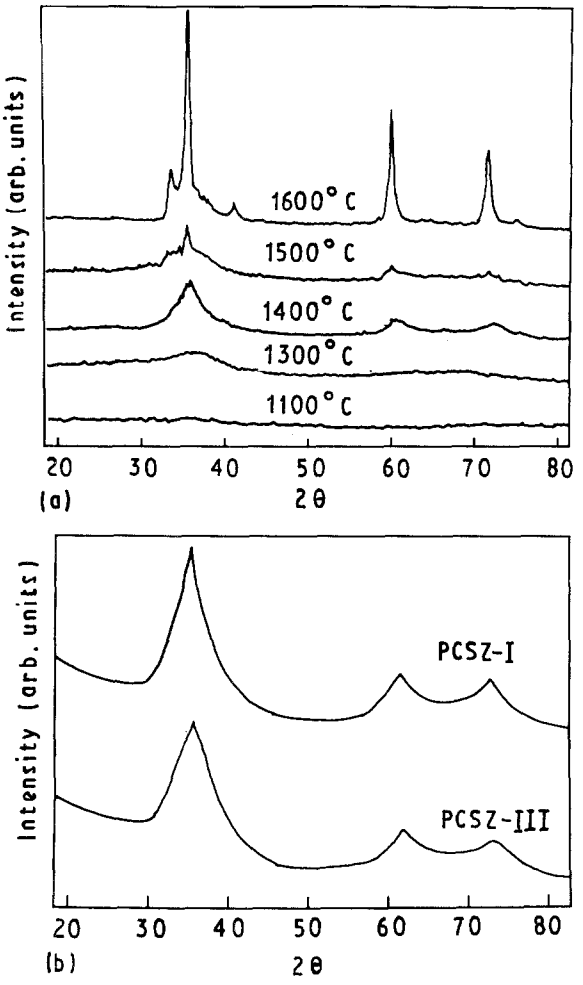

Figure 11 X-ray diffraction patterns (CuK_α) of the pyrolytic residues of the PCSZ precursors: (a) for increasing temperatures (PCSZ-I), and (b) for $\theta_p = 1400\,^\circ C$ (PCSZ-I and PCSZ-III).

whereas the other peaks were thought to correspond to hexagonal SiC polytypes. Furthermore, no significant difference is observed in the XRD patterns of the pyrolytic residues of PCSZ-I and PCSZ-III at 1400 °C (Fig. 11b).

The SiC apparent mean grain sizes were calculated from the width L of the (1 1 1) reflection (measured at mid-peak height) using Equation 1. Their variations as a function of θ_p are shown in Fig. 12. There is almost no significant increase in the mean grain size for $\theta_p < 1400\,^\circ C$, although nanocrystals of SiC could be observed and measured by transmission electron microscopy (TEM) [34]. Above this temperature, the mean grain size increases very rapidly as θ_p is raised (i.e. from 1–2 nm at 1400 °C to about 20 nm at 1600 °C). It is remarkable that the crystallization of ex-

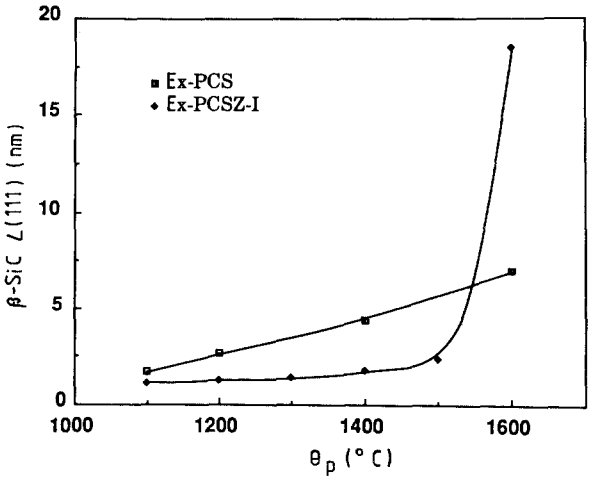

Figure 12 Variations of the apparent mean grain sizes of ex-PCSZ-I and ex-PCS pyrolytic residues as a function of pyrolysis temperature.

PCS ceramics starts about 200 °C below that of the ex-PCSZ ceramics, and this shows that the amorphous microstructure of the latter is much more stable at high temperatures than that of the former. However, for $\theta_p = 1600\,^\circ C$, the mean grain sizes of the pyrolytic residues prepared from PCS and PCSZ precursors are 7 and 20 nm, respectively. Therefore, our data show that the crystallization of ex-PCSZ ceramics is delayed with respect to that of ex-PCS ceramics but, when it occurs, the crystallization kinetics are faster.

The morphology of the external surface of the pyrolytic residues was studied by scanning electron microscopy (SEM) for increasing θ_p values (Fig. 13). For $\theta_p < 1400\,^\circ C$ the external surface of the pyrolytic residues is smooth with microporosity increasing as the degree of PSSZ/PCSZ conversion decreases. For $\theta_p = 1600\,^\circ C$, the surface morphology depends on the rate of increase of θ_p: (i) when θ_p is rapidly raised up to 1600 °C (60 °C min^{-1} or more), SiC whiskers are observed on a smooth surface; whereas (ii) when θ_p is raised slowly (10 °C min^{-1}), the external surface of the pyrolytic residue is rough and highly porous with large crystals of SiC.

3.2.8. Electrical conductivity

The electrical conductivity, measured at 500 K for the ex-PCSZ-I pyrolytic residues, dramatically increases (by seven orders of magnitude) when θ_p is raised from 850 to 1400 °C, as shown in Fig. 14. For $\theta_p = 850\,^\circ C$, the electrical conductivity significantly increases as the temperature at which it is measured is raised, a feature

TABLE VII Gas formed and weight lost during the organic/inorganic transition of PCSZ-I and PCSZ-III.

	Amount of gas (mol kg^{-1})[1]		Amount of gas (mol kg^{-1})[2]		Calc. $\Delta m/m_0$ (%)[3]	Calc. $\Delta m/m_0$ (%)[4]	$\Delta m/m_0$ (%)[5]
	H_2	CH_4	H_2	CH_4			
PCSZ-I	10.2	4.0	18.5	7.2	8.3	15.1	15.7
PCSZ-III	17.6	6.6	17.6	6.6	14.1	14.1	12

[1] as measured per kilogram of the initial sample; [2] as measured per kilogram of residue at 450 °C; [3] as calculated from the gas evolution per kilogram of initial sample; [4] as calculated from the gas evolution, per kilogram of residue at 450 °C; [5] as measured by TGA, per kilogram of residue at 450 °C.

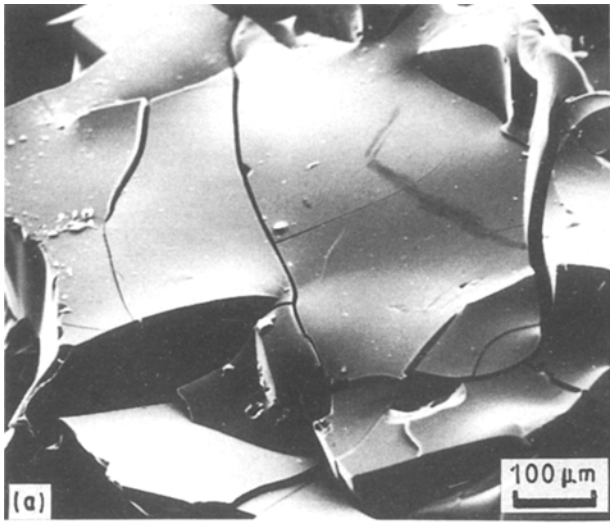

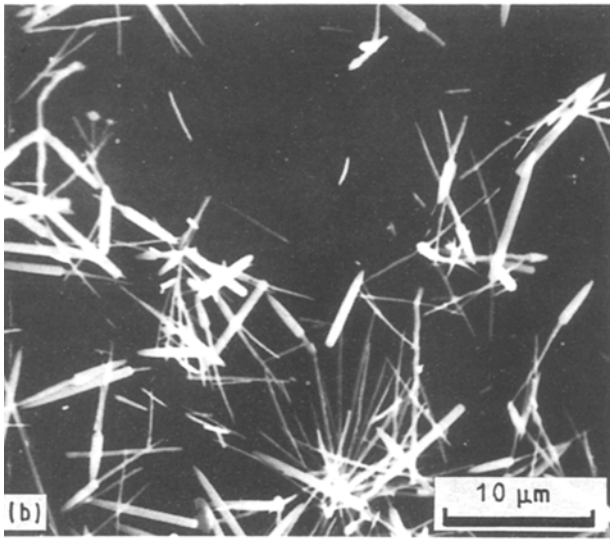

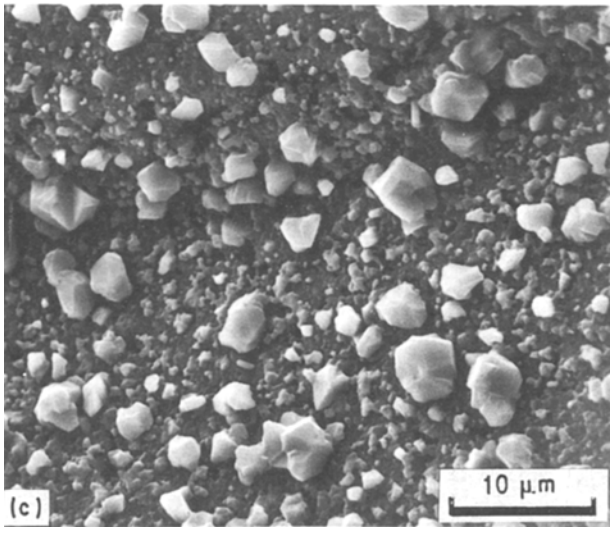

Figure 13 Morphology of the external surface of ex-PCSZ-I pyrolytic residue (a) $\theta_p = 1400\,^{\circ}C$, ramping rate $3600\,^{\circ}C\ h^{-1}$, (b) $\theta_p = 1600\,^{\circ}C$, ramping rate $3600\,^{\circ}C\ h^{-1}$; and (c) $\theta_p = 1600\,^{\circ}C$, ramping rate $600\,^{\circ}C\ h^{-1}$.

typical of semiconducting behavior (the related apparent activation energy, E_a, being equal to 0.84 eV). However, for $\theta_p = 1200\,^{\circ}C$, the temperature dependence of the electrical conductivity is less, the activation

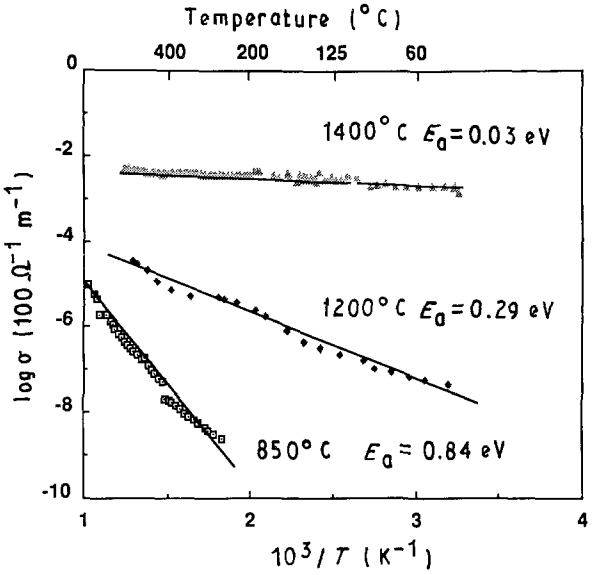

Figure 14 Thermal variations of the electrical conductivity of the pyrolytic residues of ex-PCSZ-I precursor, for $\theta_p = 850$, 1200 and 1400 °C.

energy being only 0.29 eV. Finally, for $\theta_p = 1400\,^{\circ}C$, the electrical conductivity is almost independent of the temperature at which it is measured. It is noteworthy that a similar electrical behaviour has already been reported for ex-PCS pyrolytic residues [35].

4. Discussion

The data reported in Section 3 are important for discussing the mechanisms involved in the different stages of the pyrolysis process (Section 4.1.), the effect of the PSSZ/PCSZ conversion degree on the pyrolysis process (Section 4.2.), and the influence of the pyrolysis conditions (Section 4.3.).

4.1. Mechanisms involved in the different stages of the pyrolysis process of PCSZ-I

From the experimental results, it can be inferred that the pyrolysis of PCSZ-I under an inert atmosphere proceeds according to five successive steps (Sections 4.1.1.–5) as the temperature θ_p is progressively raised.

4.1.1. For $25\,^{\circ}C < \theta_p < \theta_1$ (with $\theta_1 = 450$–$500\,^{\circ}C$)

The large weight loss which is observed within this temperature range (Fig. 4a), i.e. 45 wt %, is mainly related to: (i) the formation and evolution of low-boiling-point oligomers starting at about 300 °C (on the basis of the i.r. spectroscopy data, there is a clear similarity between these oligomers and the starting PCSZ-I precursor; moreover, the chemical composition of the pyrolytic residue at 450 °C is almost identical to that of the PCSZ-I precursor); and (ii) an evolution of both hydrogen and ammonia, but in much lower amounts. The formation of NH_3 and H_2 might be respectively related to transamination reac-

tions (2) [18, 19, 36, 37], and cleavage of Si–H and N–H bonds (3) [38]:

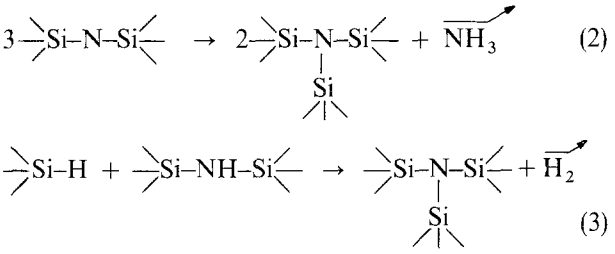

(2)

(3)

Reaction 2 explains the observed evolution of small amounts of ammonia (see Section 3.2.5.) within this temperature range as well as the almost total vanishing of the absorption bands at 3450 and 1160 cm^{-1}, respectively assigned to the valence vibration, ν(N–H), and deformation, γ(N–H), of PSZ units, –(Si–NH)–, in the i.r. spectrum of the pyrolytic residue corresponding to the upper limit of the θ_p range (Table V; Fig. 7). The observation that only minor proportions of ammonia were involved during the overall pyrolysis, leads to the assumption that the formation of Si_3N sites according to Reaction 3 is favoured.

The increase in the number of 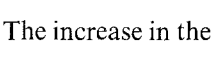 groups, which have been observed both by i.r. spectroscopy (Fig. 7) and ^{13}C NMR (CPMAS) (Fig. 10b) could be explained by the insertion of methylene groups into the Si–Si bonds according to the following Scheme, as previously described by Shiina and Kumada [30]:

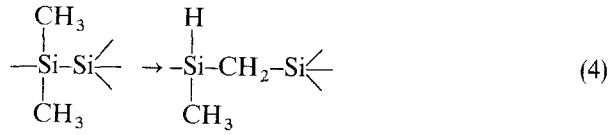

(4)

The insertion of methylene groups into Si–Si bonds according to Scheme 4 is supported by both the vanishing of the i.r. absorption band at 400 cm^{-1}, assigned to Si–Si (Fig. 7) and the decrease in the intensity of the ^{13}C NMR weak peak at − 7 p.p.m., assigned to Si–$(\underline{C}H_3)_2$-(Fig. 10b), as θ_P is raised from 25 to 500 °C. Since it does not release hydrogen, it could occur at low temperatures, i.e. for $\theta_p \leq 400$ °C (under such conditions no evolution of hydrogen was observed, as shown in Fig. 8). Alternatively, the decrease in intensity of the i.r. absorption band at 2130 cm^{-1}, assigned to Si–H, could be related to any reaction following Reaction 3 and resulting in a release of hydrogen. Finally, the decrease in the number of $\underline{Si}N_2CH$ sites and the increase in $\underline{Si}C_2N_2$ sites, which have been established on the basis of the ^{29}Si NMR analysis (Fig. 10c), could be explained by a mechanism involving condensation processes. Reactions proceeding by Reaction 3 could be favoured at high temperatures, i.e. for $400 < \theta_p < 500$ °C, since they occur with the evolution of hydrogen. However, it is thought that, within this narrow temperature range, several of these reactions might proceed with the simultaneous insertion of methylene groups into Si–Si bonds (Reaction 4).

When θ_p is raised from room temperature to 450–500 °C, the density of the residue is only slightly increased (from 1.20 to 1.25×10^3 $kg\,m^{-3}$) (Fig. 6) although there is a very large weight loss (Fig. 4) and the polymer becomes highly cross-linked. This feature could be explained by the fact that the chemical species which are vapourized are very similar in nature to those remaining in the residue, as already mentioned, and that the material remains organic.

So, it appears that three main phenomena occur in the temperature range $25 < \theta_p < 450$–500 °C: (i) condensation-cyclization processes which consume the majority of the Si–H bonds, (ii) internal rearrangements within the polymeric chains (e.g. insertion of methylene groups in the Si–Si bonds) and simultaneous progressive cross-linking of the polymer, and (iii) evolution of gaseous species (low-molecular-mass oligomers and, near the upper temperature limit, hydrogen) yielding a very large weight loss. At this stage, the material remains clearly organic.

4.1.2. *For* $\theta_1 < \theta_p < \theta_2$

When θ_p is raised from $\theta_1 = 450$–500 °C to $\theta_2 = 750$–800 °C, the PCSZ-I precursor undergoes a new weight loss which is less significant than that observed in the first temperature range, as shown in Fig. 4. This weight loss is related mainly to the formation of hydrogen and methane (Fig. 8), as shown by the fact that the weight loss calculated from the volumes of H_2 and CH_4 is almost exactly equal to that measured by TGA (Table VII). In addition to H_2 and CH_4, traces of various other gaseous organic species are also formed. This gas evolution is due to the splitting of the majority of the Si–H, Si–Me, C–H bonds progressively yielding an inorganic residue.

The occurrence of an organic/inorganic transition within this temperature range is clearly supported by i.r. and NMR data. As shown in Fig. 7, all the strong i.r. absorption bands of the as-prepared PCSZ-I precursor (e.g; ν(CH_3) at 2890 cm^{-1}; ν(SiH) at 2130 cm^{-1}; δ(CH_3Si) at 1260 cm^{-1}; δ(SiH) at 940–850 cm^{-1}) as well as those of weaker intensity (e.g. ω(Si–CH_2–Si) at 1350 cm^{-1} and δ(Si–CH_2–Si) at 1040 cm^{-1}) resulting from the PSSZ/PCSZ conversion almost totally disappear when θ_p is raised from θ_1 to θ_2. Similarly, the change occurring in the NMR spectra (Fig. 10) shows that, within this temperature range, the number of $\underline{Si}$–H, –CH_3 and $\underline{Si}N_2HMe$ sites decreases; and $\underline{Si}N_2C_2$ and $\underline{C}Si_4$ sites appear.

The mechanisms governing the formation of CH_4 and H_2 are still a matter of speculation. However, free radicals might be involved as intermediates, as previously suggested by Hasegawa and Okamura [39] in the organic/inorganic transition taking place within, approximately, the same temperature range as for PCS (at this stage of the pyrolysis of PCSZ, NH bonds are no longer present since they have been replaced by $\underline{N}Si_3$ knots during the cross-linking process at lower temperatures, thus the reactivity of the PCSZ residue is thought to be close to that of the PCS residue). We have no supplementary evidence for supporting the homolytic cleavages assumed by these authors to involve the formation of H_2 and CH_4.

The organic/inorganic transition yields an amorphous solid, which is homogenous in chemical composition. As shown in Tables IIIa, b, and IV, a very important change occurs in the elemental composition of the pyrolytic residue during the transition: (i) the hydrogen concentration dramatically decreases, as could be expected (from 61 to 25.7 at % when θ_p is raised from 25 to 850 °C); whereas (ii) those of the other elements increase by a factor of two for silicon and nitrogen (since these elements are not present in the pyrolysis gaseous species) and by a factor significantly lower for carbon, i.e. 1.52, since part of the carbon is lost as CH_4. Despite the important gas evolution within this temperature range, we have to specify that the pyrolytic residue still contains, at $\theta_p = 850$ °C, significant amounts of hydrogen (Fig. 5) and C–H organic bonds (Fig. 7), a feature which might be correlated with the residue's amorphous character.

Finally an important change occurs in the density of the material at the organic/inorganic transition. As shown in Fig. 6, the density increases from 1.25 $\times 10^3$ kg m^{-3} for the organic state ($\theta_p = 500$ °C) to 2.2 $\times 10^3$ kg m^{-3} for the inorganic state ($\theta_p = 800$ °C) as expected for a transition between a three-dimensional open network of polymeric chains and a glassy material, largely mineral, with pores of nanometer scale [34].

4.1.3. *For $\theta_2 < \theta_p < \theta_3$ (with θ_3 = 1200–1200 °C)*

The amorphous pyrolytic residue resulting from the organic/inorganic transition remains relatively stable when θ_p is raised from $\theta_2 = 750$–800 °C to $\theta_3 = 1200$–1250. However, the evolution of hydrogen (and to some extent of methane) continues to proceed, as shown in Figs 5 and 8 and Table IIIb. This has three consequences: (i) a small weight loss (Fig. 4b), (ii) an increase in the concentrations of Si, C and N in the pyrolytic residue (Table IIIb), and (iii) a regular increase in density (Fig. 6). All these phenomena suggest that some local atomic rearrangements occur in the solid which, however, remains amorphous up to about 1200 °C.

Near the upper limit of the temperature domain, i.e. when θ_p is close to 1200 °C, the amorphous pyrolytic residue begins to crystallize; this is supported by TEM data which will be published in detail elsewhere [34]. However, at this temperature this phenomenon remains limited: some crystals of β-SiC (mean size, 2 nm) as well as few basic structural units (BSUs) of free carbon [34] appear within an amorphous Si–C–N matrix – characterized by both $\underline{Si}C_2N_2$ and $\underline{Si}C_3N$ (and possibly $\underline{Si}C_4$) sites (^{29}Si NMR; Fig. 10c) – which remains the majority of the material.

For $\theta_p = 850$ °C, the pyrolytic residue exhibits a low electrical conductivity with a semiconducting character and an E_a of 0.84 eV. However, when θ_p is raised from 850 to 1200 °C, the electrical conductivity increases by more than three orders of magnitude and, simultaneously, E_a falls to 0.29 eV.

4.1.4. *For $\theta_3 < \theta_p < \theta_4$ (with $\theta_4 \approx 1400$ °C)*

When θ_p is raised from $\theta_3 \approx 1200$ °C to $\theta_4 \approx 1400$ °C, the crystallization process, which has started just below θ_3, becomes more and more important, as shown in Fig. 11 from the sharpening of the broad XRD peaks (assigned to SiC) and to a lesser extent in Fig. 7 from that of the i.r. absorption band at 850 cm^{-1} (assigned to SiC). The mean grain size of SiC increases from 2 to 5 nm for PCSZ-I samples treated for 1 h at 1200 °C and for 1 h at 1400 °C, respectively. Furthermore, the simultaneous formation of free carbon (sp^2) also proceeds in a more and more significant manner, as supported by the sharpening of the i.r. absorption band at 1100 cm^{-1}, assigned to aromatic carbon (Fig. 7). This crystallization process has also been observed by Delverdier *et al.* [34] using TEM: the SiC-crystals appear to be surrounded by cages of free carbon (more-or-less completely formed) in which the graphite planes lie parallel to the SiC-crystal facets, as shown in Fig. 15.

For $\theta_p \approx 1400$ °C, only traces of hydrogen remain in the pyrolytic residue (less than 0.2 at % Table IIIb and Fig. 5) and the density is 2.55 $\times 10^3$ kg m^{-3} (cf. a density of 2.4 $\times 10^3$ kg m^{-3} at $\theta_p = 1200$ °C). Furthermore, as shown in Table IIIb and Fig. 9, the pyrolytic residue of PCSZ-I at 1400 °C still contains a large amount of nitrogen (approximately 20 at %) which is thought to be present in the material mainly as a Si–C–N amorphous matrix, as previously discussed in Section 4.1.3.

Finally, as shown in Fig. 14, the electrical conductivity measured at 500 K, has increased to the order of a few Ω^{-1} cm^{-1} compared to 3 $\times 10^{-4}$ and approximately 10^{-7} 10^{-10} Ω^{-1} m^{-1} for $\theta_p = 1200$ and 850 °C, respectively. Moreover, the electrical conductivity becomes almost independent of the temperature at which it is measured (E_a being only 0.03 eV). For

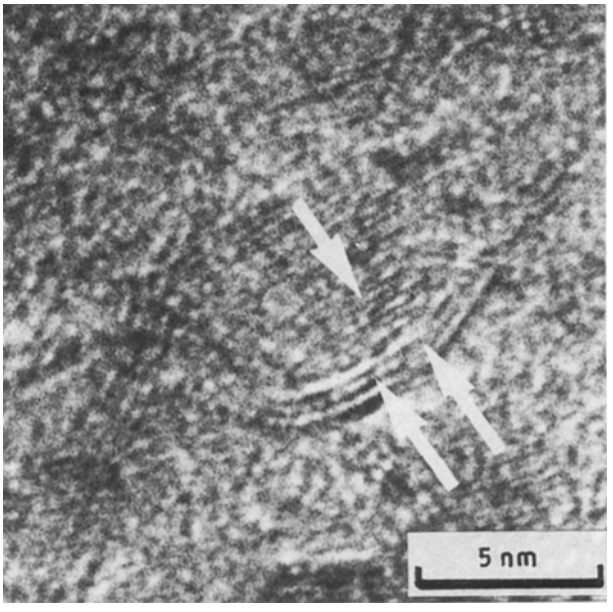

Figure 15 High resolution TEM picture (lattice-fringe mode) of the pyrolytic residue of PCSZ-I treated at 1400 °C showing: (i) β-SiC crystals (single arrow) and (ii) carbon cages (double arrow), reprinted with permission of O. Delverdier, M. Monthioux and A. Oberlin [34].

comparison, E_a for the PCSZ-I pyrolytic residue obtained at 1400 °C is close to that of an anthracene char prepared at 700 °C [41]. It is thus suggested that the change in the electrical behaviour observed when θ_p is raised from θ_3 and θ_4 can be related mainly to the growth of the dehydrogenated aromatic carbon and to its local arrangement as cage-like structures around the β-SiC crystals; the electrical conductivity could result from a hopping process occurring between these more-or-less-complete-and-interconnected cages of free carbon. A similar mechanism has been proposed previously to explain the dramatic increase in electrical conductivity which is observed in PCS pyrolytic residues as θ_p is raised [42].

4.1.5. For $\theta_p > \theta_4$ (with $\theta_4 \approx 1400$ °C)

When θ_p is raised beyond $\theta_4 \approx 1400$ °C, a second large weight loss occurs which is the result of the evolution of almost all the nitrogen present in the material (Figs. 4b and 9, and Table IIIa) and, to a lesser extent, of carbon monoxide. As a result of this decomposition process, assigned to the Si–C–N amorphous matrix, important changes occur in the pyrolytic residue: (i) its concentration of elemental carbon significantly increases (from 32 to 50 at % at 1400 and 1600 °C, respectively) whereas that of elemental silicon is not changed (so there is a loss of silicon in the gas phase), (ii) its density increases again (its value being 2.75 $\times 10^3$ kg m^{-3} for $\theta_p = 1600$ °C), and (iii) both the number and size of the β-SiC crystals are increased (Fig. 12). The latter observation was also made by Delverdier *et al.* on the basis of a high resolution TEM (HRTEM) study, as shown in Fig. 16 [34]. Interestingly, the carbon surrounding the large β-SiC crystals now consists of carbon BSUs randomly oriented (instead of cage-like structures in which the graphite planes are parallel to the β-SiC facets, observed at a lower θ_p). Finally, SiC whiskers are formed on the surface of the sample (Fig. 13).

The phenomena observed during the pyrolysis of PCSZ-I for $1400 < \theta_p < 1600$ °C can be explained as follows (i) the Si–C–N amorphous matrix undergoes a decomposition process yielding mainly SiC and free carbon with evolution of nitrogen and gaseous silicon and/or SiO; and (ii) the latter reacts, firstly, within the solid itself with the carbon cages forming disoriented BSUs and secondly, with carbon-containing species from the atmosphere of the furnace to give SiC whiskers on the external surface of the sample. Thus for $\theta_p = 1600$ °C, the pyrolytic residue of PCSZ-I is mainly a mixture of β-SiC crystals and free carbon with trace amounts of other atoms (i.e. 3 at % of N, 3 at % of O and less than 0.1 at % of H).

4.2. Effect of the PSSZ/PCSZ conversion degree on the organic/inorganic transition and the nature of the pyrolytic residue

The data reported in Section 3 on the pyrolysis of PCSZ-I–III, show that the influence of the PSSZ/PCSZ conversion degree in the as-prepared

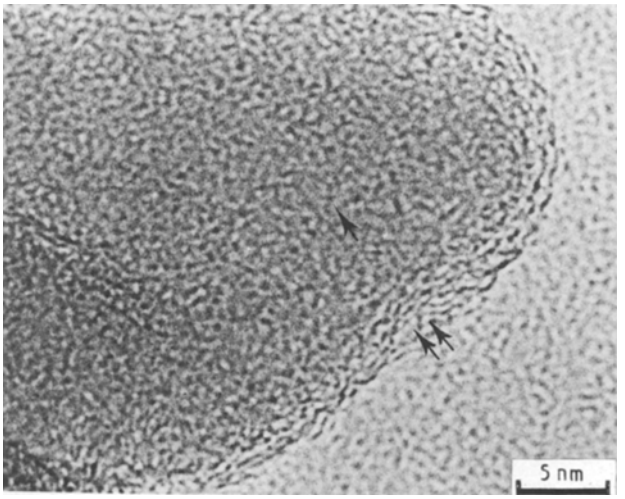

Figure 16 TEM picture (bright-field mode) of the pyrolytic residue of PCSZ-I obtained at 1600 °C showing a large crystal of β-SiC (single arrow) surrounded by disoriented BSUs of carbon (double arrow), reprinted with permission of O. Delverdier, M. Monthioux and A. Oberlin [34].

precursors is effective in the first stages of the pyrolysis process (i.e. for $\theta_p < \theta_2$) and negligible (if there is any) in the last stages (i.e. for $\theta_p > \theta_2$).

For $\theta_p < \theta_1$ (with $\theta_1 = 450$–500 °C), the importance of the weight loss, which is related to the vapourization of low-molecular-weight oligomers, depends directly on the PSSZ/PCSZ conversion degree in the as-prepared materials: it is very large (i.e. 46 wt %) for (PCSZ-I), very small for PCSZ-III and is 22 wt % for PCSZ-II (Fig. 4). As a result, there is a little change in the i.r. spectrum of PCSZ-III when θ_p is raised from 25 to 500 °C whereas there is, within the same temperature range, a decrease in the intensity of the ν(Si–H) absorption band and simultaneously an increase in that of the ω(Si–CH_2–Si) absorption band. This can be explained by the fact that the methylene-group insertions into the Si–Si bonds, which occurs in PCSZ-I when θ_p is raised from 25 to 500 °C, have already taken place during the preparation of the precursors, partially for PCSZ-II and to a very large extent for PCSZ-III. Thus, the i.r. spectrum of PCSZ-I for $\theta_p = 450$–500 °C, on the one hand, and that of PCSZ-III, on the other hand, are quite similar.

For $\theta_1 < \theta_p < \theta_2$ the second weight loss increases as the degree of PSSZ/PCSZ conversion becomes more pronounced, at least when it is calculated with respect to the initial sample mass, m_0, (ranging from 8.5 wt % for PCSZ-I to 12 wt % for PCSZ-III; Fig. 4). However, when the weight loss is calculated with respect to the mass m_1 of pyrolytic residue at 450 °C, the relationship is reversed (the values of $\Delta m/m_1$ ranging from 19.7 wt % for PCSZ-I to 12 wt % for PCSZ-III). Thus, it is again the precursor with the highest degree of PSSZ/PCSZ conversion, in the as-prepared state, which undergoes the lowest relative weight loss within the θ_1–θ_2 temperature range, in agreement with the analysis data of the formed gases (Fig. 8).

The fact that the evolution of H_2 and CH_4 occurs at a higher temperature in PCSZ-III than in PCSZ-I could be because the gas flow in this temperature

range, 350–450 °C, is almost achieved during the thermolysis of PCSZ-III.

For $\theta_p > \theta_2$, the phenomena observed during the pyrolysis of both PCSZ-I and PCSZ-III are very similar: it appears that the effect of the PSSZ/PCSZ conversion degree on the last stages of the pyrolysis, if there is any, is weak and that the elemental compositions of both the pyrolytic residues at 1600 °C are the same, as shown in Tables III and IV.

4.3. Effect of the pyrolysis conditions

Between $\theta_p = 850$ °C and 1400 °C, no apparent effect of the temperature-increase rate (within the range 1–50 °C min^{-1}) was observed. On the other hand, beyond this limit, the decomposition process of the Si–C–N amorphous matrix was found to be dependent on the temperature-increase rate, as shown by the morphology of the external surface of the pyrolytic residues (Fig. 13).

5. Conclusions

From the data reported in this paper, it appears that the pyrolysis under an inert atmosphere of the PCSZ precursors to Si–C–N ceramics prepared from PSSZ copolymers can be analysed on the basis of five temperature domains.

1. From room temperature to 450–500 °C, a first weight loss occurs, and is related to the volatilization of low-molecular-mass oligomers. Its values depend directly upon the PSSZ/PCSZ conversion degree of the as-prepared material. The weight loss is either very large (up to almost 50 wt %) when the conversion degree is low or nil when the degree of conversion is high.

2. An organic/inorganic transition takes place between 450–500 °C and 750–850 °C. It yields an amorphous Si–C–N residue containing a significant amount of hydrogen, while evolution of both hydrogen and methane is observed.

3. Within a rather large temperature range, i.e. from 750–850 °C to 1200–1250 °C, the majority of the residual hydrogen is progressively released with a slight increase in the density of the pyrolytic residue. Within this temperature range, the material remains amorphous and it exhibits a semiconducting electrical behavior.

4. Within a rather narrow temperature range, i.e. from 1200–1250 °C to 1400 °C, the amorphous silicon carbonitride undergoes a crystallization process (whose kinetics becomes significant near 1400 °C) giving rise to β-SiC crystals surrounded by cage-like structures of free-carbon BSUs whose graphite planes lie parallel to the SiC crystal facets. Otherwise evolution of the residual hydrogen, occurs and, as a result, the electrical conductivity significantly increases.

5. Finally, beyond 1400 °C, a decomposition process occurs within the amorphous silicon carbonitride with evolution of both nitrogen and silicon (Si or SiO); this is responsible for a second and important weight loss. At 1600 °C, the pyrolytic residue is a mixture of large β-SiC crystals and free carbon.

Therefore, it appears that the pyrolytic Si–C–N solids derived from PCSZ precursors exhibit an amorphous state which is more stable with respect to temperature than that previously reported for the pyrolytic Si–C–O solids derived from PCS precursors.

Acknowledgements

This study has been performed within a national research program supported by CNRS, Direction des Recherches et Etudes Techniques (DRET), Rhône-Poulenc (RP) and Société Européenne de Propulsion (SEP). The assistance of Mrs. Chassagneux (RP) for the gas analyses, M. M. Dordor and Marquestaux from Laboratoire de Chimie du Solide (LCS) for the electrical measurements is acknowledged. The authors are indebted to P. Olry (SEP) for valuable discussions and to O. Delverdier, M. Monthioux and A. Oberlin for their contribution to the analysis of the data and for letting them use previously unpublished HRTEM pictures of materials in the present study.

References

1. B. SARUHAN, M. J. POMEROY and S. HAMPSHIRE, in "Non-oxide technical engineering ceramics", edited by S. Hampshire (Elsevier Applied Science, London and New York, 1986) p. 69.
2. J. DELMONTE, in "Technology of carbon and graphite fiber composites", edited by (Van Nostrand Reinhold, New York, 1981) p. 41.
3. S. AWASTHI and J. L. WOOD, *Adv. Ceram. Mater.* **3/5** (1988) 449.
4. W. VERBEEK, US Patent 3,853.567, December (1974).
5. P. POPPER, *Brit. Ceram. Res. Ann. Special Publ.* **57** (1967) p. 99.
6. S. YAJIMA, *J. Amer. Ceram. Soc.* **59**/7-8 (1976) 324.
7. L. MAYA, *J. Amer. Ceram. Soc.* **71**/12 (1988) 1104.
8. K. B. SCHWARTZ and Y. D. BLUM, *Mater. Res. Soc. Symp.* **73** (1986) 483.
9. W. S. REES and D. SENFERTH, *J. Amer. Ceram. Soc.* (1988) C 194.
10. R. W. RICE, *Ceram. Bull.* **62**/8 (1983) 889.
11. D. SEYFERTH, *Ann. Chem. Soc.* **360** (1988) 124.
12. K. OKAMURA, *Composites* **18**/2 (1987) 107.
13. R. NASLAIN, "Introduction to Composite Materials", Vol. 2, Metallic and Ceramic Matrix Composites (in French), (Editions CNRS/IMC, Bordeaux, 1985).
14. E. FITZER, *High Temp. Soc.* **13** (1980) 149.
15. S. YAJIMA, "Handbook of Composites, "Vol. 1, Strong Fibers edited by W. Watt and B. V. Peron (Elsevier Science, New York, 1985).
16. K. OKAMURA, M. SATO, T. MATSUZAWA and Y. HASEGAWA, *ACS Polym. Preprint* **25**/1 (1984).
17. J. LIPOWITZ, H. A. FREEMAN, R. T. CHEN and E. R. PRACK, *Adv. Ceram. Mater.* **2** (1987) 121.
18. Y. D. BLUM, K. B. SCHWARTZ and R. M. LAINE, *J. Mater. Sci.* **24** (1989) 1707.
19. NEE SUN CHOONG KWET YIVE, R. CORRIU, D. LECLERC, P. H. MUTIN and A. VIOUX, *New J. Chem.* **15** (1991) 85.
20. E. BOUILLON, R. PAILLER, R. NASLAIN, J. P. PILLOT, M. BIROT, E. BACQUE and P. V. HUONG, *Chem. of Mat.* **3**/2 (1991) 356.
21. J. P. PILLOT, C. RICHARD, J. DUNOGUES, M. BIROT, R. PAILLER, D. MOCAER, R. NASLAIN, P. OLRY and E. CHASSAGNEUX, *l'Industrie Céramique* **48** (1992) 867.
22. E. BACQUE, J. P. PILLOT, J. DUNOGUES and P. OLRY, European Patent 296028 (1988).
23. E. BACQUE, J. DUNOGUES, C. BIRAN, P. OLRY and J. P. PILLOT, French Patent 2589037 (1986).

24. C. LAFFON, P. LAGARDE, A. M. FLANCK, R. HAGEGE, P. OLRY, J. COTTERET, S. DIXMIER, M. LARIDJANI, A. P. LEGRAND and B. HUMELLE, *J. Mater. Sci.* **24** (1989) 1503.
25. C. GERARDIN and F. TAULELLE, Internal Report (1990).
26. R. E. WASYLISHEN and C. A. FYFE, in "Solid state NMR for chemists" edited by C. A. Fyfe, *Annu. Rep. N.M.R. Spectrosc.* **12** (1982) 1.
27. S. YAJIMA, J. HAYASHI, M. OMORI and K. OKAMURA, *Nature* **261** (1976) 683.
28. J. GAUL, European Patent 0075826 (1982).
29. C. GERARDIN, F. TAULELLE, C. RICHARD, J. P. PILLOT and J. DUNOGUES, Unpublished work.
30. K. SHIINA and M. KUMADA, *J. Org. Chem.* **23** (1958) 139.
31. Y. HASEGAWA, M. IIMURA, S. YAJIMA, *J. Mater. Sci.* **15** (1980) 720.
32. E. BOUILLON, D. MOCAER, J. F. VILLENEUVE, R. PAILLER and R. NASLAIN, "Matériaux Composites pour Applications à Hautes Températures", edited by R. Naslain, J. Lamalle and J. L. Zulian (AMAC/CODEMAC, Bordeaux 1990).
33. S. M. JOHNSON, R. D. BRITTAIN, R. H. LAMOREAUX and D. J. RANCLIFFE, *J. Am. Ceram. Soc.* **71**/3 (1988) C-132.
34. O. DELVERDIER, Internal Report (1989).
35. E. BOUILLON, F. LANGLAIS, R. PAILLER, R. NASLAIN, F. CRUEGE, P. V. HUONG, J. C. SARTHOU, A. DELPUECH, C. LAFFON, P. LAGARDE, M. MONGHIOUX and A. OBERLIN, *J. Mater. Sci.* **26** (1991) 1333.
36. U. WANNAGAT, *Adv. Inorg. Chem. Radiochem.* **6** (1964) 225.
37. B. J. AULETT, *Organomet. Chem. Rev.* **3** (1968) 151.
38. M. ARAI, SAKURADA and T. ISODA, *Polym. Prefer.* **28** (1987) 407.
39. Y. HASEGAWA and K. OKAMURA, *J. Mater. Sci.* **18** (1983) 3633.
40. R. CORRIU, Internal Report (1989).
41. F. CARMONA, PhD thesis number 509, Bordeaux (1976).
42. M. MONTHIOUX, A. OBERLIN, E. BOUILLON, *Composite Sci. and Tech.* **37** (1990) 21.

Received 17 August
and accepted 9 September 1992